Engineering Geology 235 (2018) 39–52

Contents lists available at ScienceDirect

Engineering Geology

journal homepage: www.elsevier.com/locate/enggeo

Integration of ground-based radar and satellite InSAR data for the analysis of an unexpected slope failure in an open-pit mine

Tommaso Carlà[a,b,*], Paolo Farina[c], Emanuele Intrieri[b], Hakki Ketizmen[d], Nicola Casagli[b]

[a] Regional Doctoral School of Earth Sciences, University of Florence, Via La Pira 4, 50121 Firenze, Italy
[b] Department of Earth Sciences, University of Florence, Via La Pira 4, 50121 Firenze, Italy
[c] Geoapp s.r.l., Academic spin-off of the University of Florence, Largo E. Fermi 2, 50125 Firenze, Italy
[d] Mining Engineer, Turkey

ARTICLE INFO

Keywords:
Slope failure
Slope monitoring
Satellite InSAR
Ground-based radar
Open-pit mine
Tertiary creep

ABSTRACT

On 17 November 2016, an unexpected slope failure occurred in an undisclosed copper open-pit mine. The nature of the event urged for a thorough back-analysis of slope monitoring data in order to assess its size and temporal evolution, and to determine whether precursors potentially able to anticipate the failure were present. To this aim, satellite InSAR data spanning over the final 9 months before the event were, in retrospect, acquired and coupled with measurements from a ground-based radar that was in use at the time of the failure. Although progressive deformation was detected by the ground-based radar in correspondence of the two uppermost benches in the pit, the satellite InSAR data revealed that the vast majority of the instability actually involved a large part of natural slope above the mine crest. This sector was not visible by the ground-based radar. Thanks to the short revisit time of the Sentinel-1 mission, clear slope accelerating creep was observed for the first time in satellite InSAR measurements over an open-pit mine. The delimitation of the area featuring accelerating creep behavior matched remarkably the source area of the failure as mapped in the field after the event. Considerations on the volume of the instability and on the development of the failure process (both in space and time) were consequently derived. The results provided a clear example of the value of jointly using ground-based and satellite interferometry to reduce the uncertainties inherent to the identification and characterization of impending catastrophic slope failures.

1. Introduction

Slope failures, which involve physical detachment and consequent collapse of rock and/or earth material at local or global scale, are geohazards with great destructive power. An effective evacuation strategy is strictly related to the implementation of comprehensive monitoring programs able to detect the size of the slope sectors affected by instability, coupled with methods aimed at deriving reliable predictions of the time of failure. The analysis of the trend of slope displacement, velocity, and acceleration with time is usually emphasized, since these parameters are considered the best indicators of ongoing failure processes. Identifying phases of "progressive" deformation, during which the slope displaces at an accelerating rate up to the point of failure (i.e. accelerating creep), is of crucial importance for any early warning system (Zavodni and Broadbent, 1978; Eberhardt, 2008; Michoud et al., 2013).

Estimating the time of slope failure is in fact typically obtained by fitting empirical functions to curves of accelerating displacements with time (Federico et al., 2012; Intrieri and Gigli, 2016). Models related to the accelerating creep theory are mostly solved graphically through the use of the inverse velocity method, according to which the time of failure corresponds to the point of intersection on the abscissa of the extrapolated trend in a 1/velocity vs. time plot (Fukuzono, 1985; Voight, 1988; Voight, 1989; Petley et al., 2002; Crosta and Agliardi, 2003; Sornette et al., 2004). In common practice, such trend is frequently associated with a best-fit linear regression of the inverse velocity data (Petley et al., 2005; Rose and Hungr, 2007; Carlà et al., 2016a).

Within this context, radar interferometry from both ground-based and satellite platforms has surfaced as one of the most effective approaches to measure slope displacements (Casagli et al., 2010; Casagli et al., 2017). By assessing the phase change of the back-scattered signal between adjacent acquisitions that is due to movement of the ground surface, it does not require the installation of physical reflectors. Although relying on the same basic principles, data from the two types of system present different properties (Monserrat et al., 2014; Crosetto

* Corresponding author at: Regional Doctoral School of Earth Sciences, University of Florence, Via La Pira 4, 50121 Firenze, Italy.
E-mail address: tommaso.carla@unifi.it (T. Carlà).

https://doi.org/10.1016/j.enggeo.2018.01.021
Received 1 September 2017; Received in revised form 8 December 2017; Accepted 22 January 2018
Available online 31 January 2018

et al., 2016).

Ground-based radar interferometry provides advantages such as extremely high frequency of monitoring (in the order of one acquisition every few minutes) and detailed line-of-sight (LOS) slope coverage area in the form of 2D deformation maps (Dick et al., 2015). It is commonly used for applications in both natural and engineered slopes at relatively small scale, and is regarded as a fundamental tool for the design of landslide early warning systems and for detecting phases of accelerating displacement that may ultimately lead to failure (Tarchi et al., 2003; Antonello et al., 2004; Luzi et al., 2006; Herrera et al., 2009; Espinosa et al., 2013; Farina et al., 2013; Farina et al., 2014; Atzeni et al., 2015). Concerning open-pit mines, where comprehensive monitoring programs are usually undertaken (Read and Stacey, 2009; Vaziri et al., 2010), and the conditions for the rapid development of instabilities are favored by frequent changes in slope geometry and loading conditions (Crosta et al., 2017), the literature reports several cases of catastrophic failures that were successfully predicted thanks to the information supplied by ground-based radar devices (Armstrong and Rose, 2009; Doyle and Reese, 2011; Dick et al., 2015).

Satellite InSAR is commonly used for a variety of purposes related to mass movements, such as landslide mapping, monitoring, modeling and, through time series analysis, for the identification of changes in deformation rates (Berardino et al., 2003; Hilley et al., 2004; Catani et al., 2005; Strozzi et al., 2005; Colesanti and Wasowski, 2006; Farina et al., 2006; Righini et al., 2008; Herrera et al., 2011; Cigna et al., 2013; Tofani et al., 2013; Komac et al., 2015; Carlà et al., 2016b; Raspini et al., 2017). The long revisit time, as well as the lack of regularity in acquisitions performed in the same mode, has been the main factors that prevented the use of the first generations of satellite InSAR sensors as an operational tool in landslide emergency management (Casagli et al., 2010). However, over the last decade, the launch of new radar satellite missions has now given the opportunity to overcome such limitation. In this sense Wasowski and Bovenga (2014), following the introduction of the new generation of InSAR sensors, envisioned the combined use of satellite interferometry and ground-based geotechnical monitoring as a tool for the early detection and warning of potential slope failures, and recognized the prospect of significant breakthroughs and improvements in the understanding and modeling of slope instability processes. Most recently, Intrieri et al. (2017) detected pre-failure accelerating creep of the catastrophic Maoxian landslide in China by means of Sentinel-1 InSAR data.

Few attempts at combining satellite and ground-based InSAR for landslide investigation are available in the literature (Corsini et al., 2006; Bardi et al., 2014; Frodella et al., 2016). In these cases, a synergic use of the two monitoring techniques was proposed. This consists of a pre-failure analysis of possible landslide precursors carried out with satellite InSAR, and of a post-event real-time monitoring of the slope displacements with a ground-based radar for two landslides located in Italy. The approach enabled to obtain useful information on the ground displacement measurements, with high precision and improved spatial and temporal resolution.

The object of this paper is the back-analysis of a large slope failure that occurred on 17 November 2016 in an undisclosed copper open-pit mine. Images of the failure are presented in Fig. 1 (note the presence of several trucks and excavators in the first photo to appreciate the scale of the phenomenon). Even though a ground-based radar was in operation at the pit, size and timing of the failure were unforeseen, and several casualties were counted in consequence of the incident. A thorough review of slope monitoring data was therefore undertaken to evaluate the properties of the event and of its precursors, as well as to determine the reasons behind its unexpected nature. Ground displacements measured by the Sentinel-1 satellites over the mine site were used to complement the dataset produced in near real-time by the ground-based radar. Following the recent advancements in satellite InSAR monitoring, clear pre-failure slope accelerating creep was observed for the first time in an open-pit mine in data captured with such technique.

Fig. 1. (a) Photo of the slope failure and (b) detail of the head scarp.

In retrospect, the joint analysis allowed to derive considerations on volume, development of the main rupture surface, driving factor, and predictability. The increased value of integrating ground-based and satellite radar interferometry to identify and characterize impending catastrophic slope failures was thus highlighted.

2. Case study

On 17 November 2016, an unforeseen large slope failure occurred in a copper open-pit mine, causing several casualties among the mine workers that were operating in the area. Name and location of the mine, as well as more details on the topographical and geological setting than the ones given below, cannot be disclosed for confidentiality reasons. Fig. 2 evidences the change in topographic elevation after the failure, as observed within the boundaries of the instability based on the difference between a pre- and post-event Digital Elevation Model obtained from UAV photogrammetry (contour lines are relative to the post-failure topography). Positive values indicate lowering of the ground surface, whereas negative values correspond to an increase in elevation. Based on such information, the instability can be divided into three main sectors:

1. a detachment zone at the top (roughly above the 1550 m a.s.l. contour line);
2. a primary accumulation zone in the middle (roughly between the 1550 m a.s.l. and 1500 m a.s.l. contour lines);
3. a secondary accumulation zone at the bottom, where only a thin layer of spread loose debris was deposited (hence the limited change in topographic elevation).

The external boundaries of the instability were defined by the mine engineers through field surveys carried out in the aftermath of the event (length of the red polygon in Fig. 2 is approximately 400 m, and width

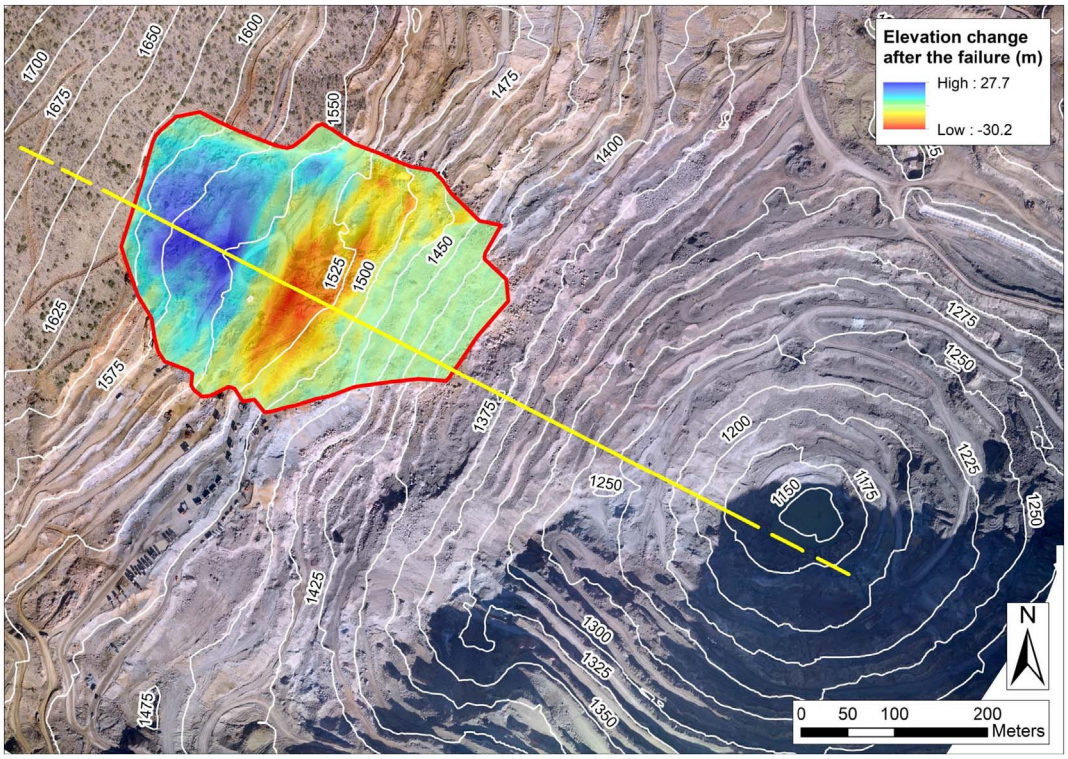

Fig. 2. Change in topographic elevation within the area of the failure. Contour lines refer to the post-failure topography. The full length of the profile trace of the cross-section in Fig. 4 is not shown because of the limited area coverage of the underlying aerial photo.

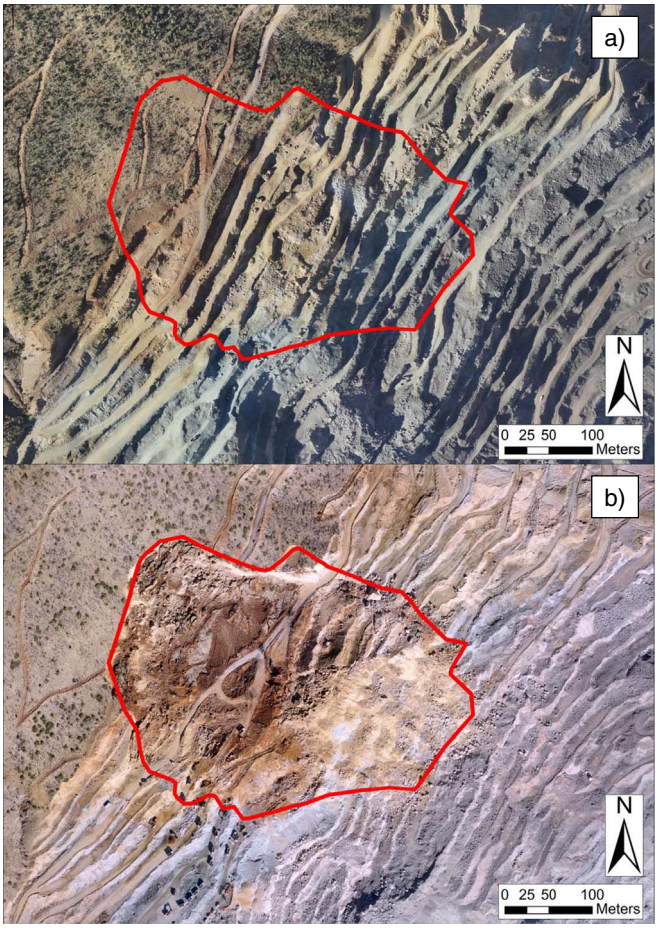

Fig. 3. Aerial photo of the failure area (a) before and (b) after the event.

ranges from 150 to 300 m). The failure affected the two uppermost benches in the NW sector of the mine, along with a large portion of adjacent natural slope above the pit crest, where the bedrock is covered by a superficial cover of loose material (Fig. 1). The average slope angle in this sector was 27.4°; the volume of the moving mass was initially estimated at 410000 m^3 based on the difference between the two DEMs. Fig. 3 shows aerial photos of the study area before and after the failure.

The schematic geological setting of the mine is shown in Fig. 4 (see Fig. 2 for location of the profile trace of the cross section). A major thrust fault separates a thick sedimentary sequence of limestone and dolomite from an area dominated by fine-grained igneous rocks, occasionally interbedded with oceanic sedimentary deposits. Spilite, resulting from the metasomatic alteration of oceanic basalts, is the most recurrent rock-type among the units in the footwall of the thrust and is the source of the ore deposit. Ore minerals include pyrite, chalcopyrite, galenite, bornite, chalcocite, and others. The failure involved the two uppermost benches in the pit, in proximity of the thrust fault. These benches were excavated through a formation of slope debris made of recrystallized limestone blocks.

3. Slope monitoring data

A ground-based interferometric radar was in use for measuring pit-slope displacements at the time of the failure. This was positioned in the SSE corner of the mine, thus giving a comprehensive slope coverage from North to West (Fig. 5). The interval of available monitoring data includes the last three weeks prior to the failure (i.e. from 27 October to 17 November 2016), featuring an acquisition frequency of one measurement every 6 min. Voids in the radar spatial coverage over the instability, apart from the horizontal flat sections of the benches not visible by the instrument because of the unfavorable looking geometry, were most likely due to the production works being carried out in that area during the mentioned reference period. For this reason, significant disturbance on the local quality of the measurements was expected by the mine personnel in charge of monitoring. Moreover, as the system

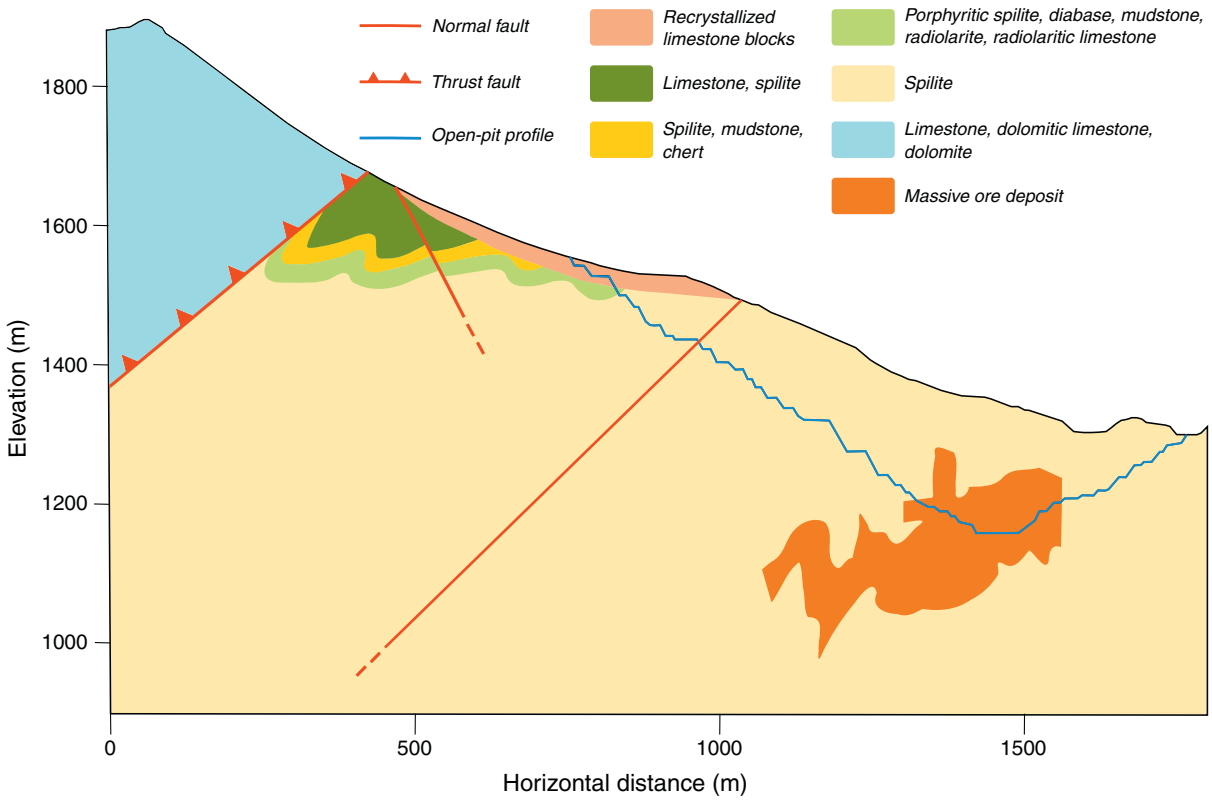

Fig. 4. Schematic geological cross section of the pit (see Fig. 2 for location of the profile trace). (For interpretation of the references to color in this figure, the reader is referred to the web version of this article.)

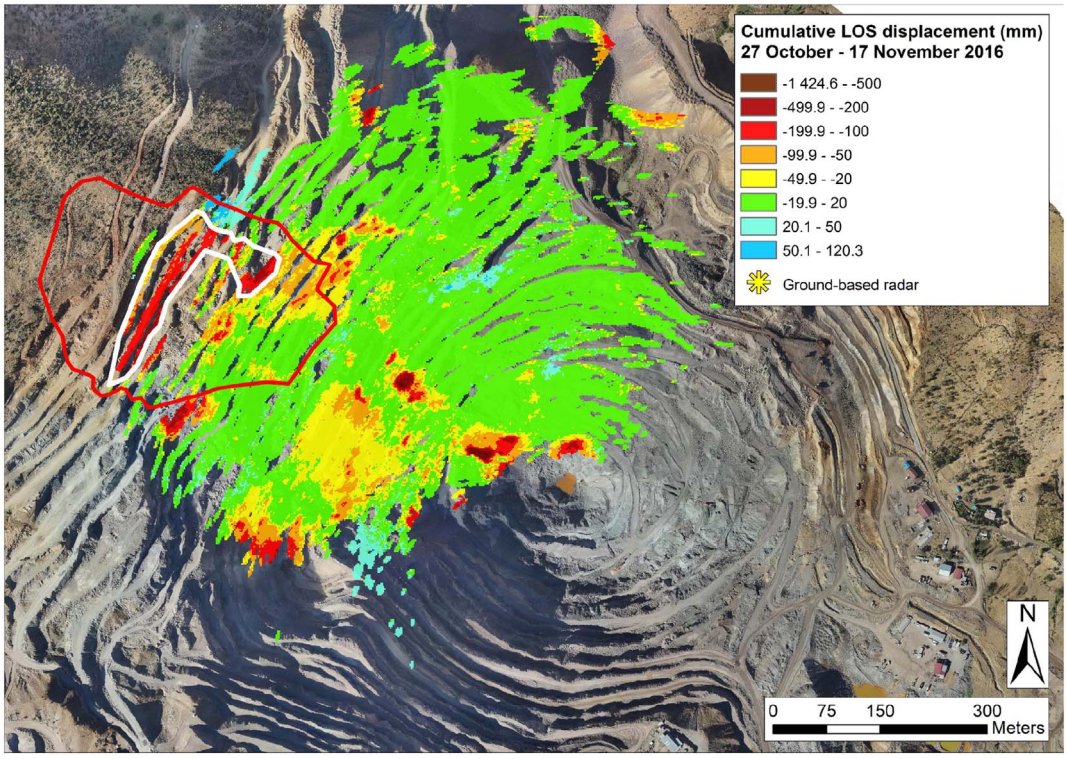

Fig. 5. Cumulative LOS deformation map produced by the ground-based radar relatively to the period 27 October – 17 November 2016. Negative values indicate movement towards the sensor. The white polygon highlights the area characterized by accelerating creep (see Section 4.1). (For interpretation of the references to color in this figure, the reader is referred to the web version of this article.)

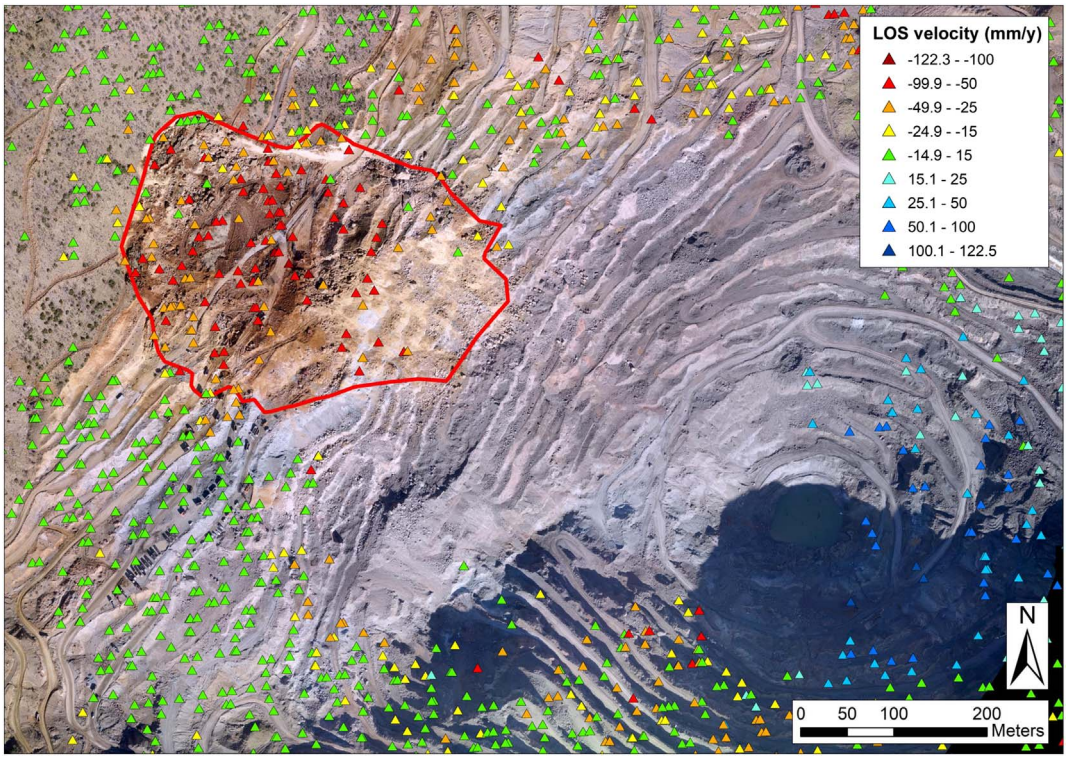

Fig. 6. Satellite InSAR data acquired in ascending geometry over the study area from 19 February to 21 November 2016. Negative values indicate movement away from the sensor. See Fig. 8 for details on the satellite looking angle. (For interpretation of the references to color in this figure, the reader is referred to the web version of this article.)

was set up to maximize detection of the displacements of the mine slopes, the radar coverage did not extend above the pit crest. Specifically, no information could be retrieved relatively to the slope sector above the top bench situated at an elevation of approximately 1550 m a.s.l (Fig. 2). As a result most of the detachment zone of the 17 November 2016 slope failure was not visible by the radar. Still, several deforming areas associated with large LOS cumulative displacements can be observed (Fig. 5, where negative values indicate movement towards the sensor). Specifically, the most spatially consistent and intense slope movement is identified in correspondence of the two uppermost benches of the pit.

In Figs. 6 and 7, satellite InSAR measurements of ground deformation over the open-pit mine, obtained through the processing of 28 Sentinel-1 images by means of the SqueeSAR algorithm (Ferretti et al., 2011), are presented. The time interval of monitoring spans from 19 February to 21 November 2016, i.e. 4 days after the failure. Satellite revisit time was 12 days up until 28 September 2016, and then shifted to 6 days in the last part of the monitoring period thanks to the availability of Sentinel-1B data. It follows that the last acquisition prior to the failure was made on 15 November 2016, i.e. 2 days before the event. Data were acquired in both ascending (Fig. 6) and descending geometry (Fig. 7), however the latter are of little value because of the lack of a significant number of point scatterers identified on the ground in the area of interest. This was caused by layover effects determined by the unsuitable looking geometry of the descending orbit. Conversely, the ascending dataset (details on the satellite looking angle in Fig. 8) provides very good coverage of measuring points both over the instability and in its surroundings, with the exception of the lower part of the secondary accumulation zone and further downslope towards the bottom of the pit. In sharp contrast with the adjacent stable areas, high average LOS velocities (up to −122.3 mm/year, where in this case negative values indicate movement away from the sensor) can be observed over the entire slope sector affected by the failure. The spatial distribution of these high velocities is extremely consistent with the limits of the instability (as mapped through the difference of the DEMs).

4. Analysis of the slope displacements

Defining the dominant patterns of movement is of crucial importance for the analysis of slope monitoring data, and, when looking to identify precursors to failure, is typically concentrated upon the nature of the periods of acceleration (Petley et al., 2005). As previously mentioned, the best known evidence of an ongoing failure process consists of a progressive phase of deformation in the form of accelerating creep. The characteristics of the ground-based radar and satellite InSAR datasets, and the predictability of the failure, were thus investigated accordingly.

4.1. Ground-based radar data

Fig. 5 details the cumulative slope displacements detected by the ground-based radar in the area of the instability prior to the failure. Given the extremely large number of pixels, it is not practically feasible to perform a specific classification of the type of deformation trend for each one of these measuring points, but rather is more convenient to identify the most important sectors within the deformation map that display similar behavior. In particular, the white polygon delimits the radar data featuring accelerating creep, that therefore can be associated with an ongoing process of failure. This involves a surface of approximately 16,000 m^2 (including the voids caused by lack of radar coverage) mostly situated in correspondence of the main accumulation zone and at the bottom of the detachment zone (as introduced in Fig. 2). Total LOS displacements range between 100 mm and 250 mm. Almost no other data are available further upslope. As a result, the limited size of the area in accelerating creep constitutes an important obstacle to a proper assessment of the size of the failure, whose boundaries identify a surface of approximately 95,000 m^2.

Fig. 5 also features some ambiguous data in proximity of the outer limits of the deformation map. Specifically:

- a 60-m long section of the pit crest characterized by no signs of

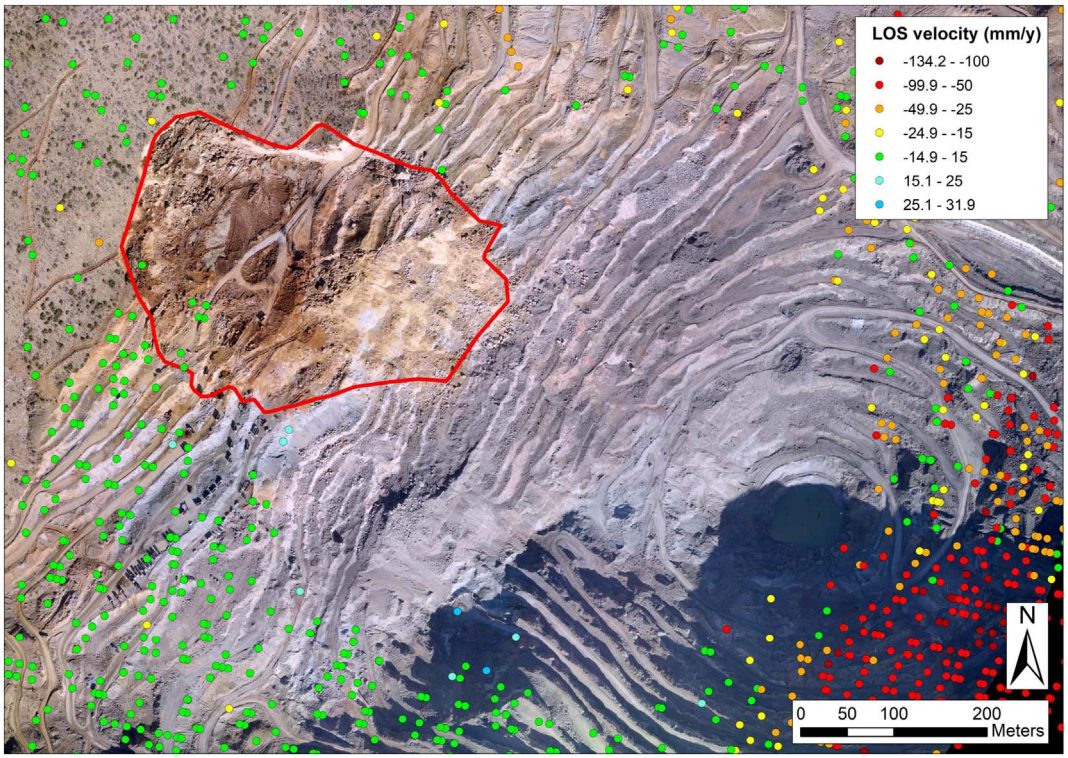

Fig. 7. Satellite InSAR data acquired in descending geometry over the study area from 19 February to 21 November 2016. Negative values indicate movement away from the sensor. (For interpretation of the references to color in this figure, the reader is referred to the web version of this article.)

deformation;

- a larger sector on the eastern side of the failure showing movements away from the sensor that are not compatible with any reasonable direction of slope movement.

These elements may be considered artifacts generated at the edges of the slope coverage area by the processing of the radar images, and could have been misleading for identifying the extension of the detachment zone above the pit crest and for correctly estimating the proportions of the failure during near real-time monitoring.

On the other hand, Fig. 9 describes the average LOS cumulative displacement-time curve of such accelerating area (i.e. derived by averaging the measurements of all the pixels therein included). This appears to be characterized by a classic exponential shape, indicating a progressive increase of slope velocity. The latter point is clearly testified in the relative velocity-time curve for the last week before the failure, as obtained by smoothing data through a 1-day running average.

Based on such plots, it can be assessed that the failure developed over a relatively long period of time, which may broadly correspond to the interval of monitoring (and possibly extend even further back in time). The final and decisive increase of slope velocity is however observed to initiate quite abruptly roughly 24 h before the failure, with values that exceeded 1 mm/day starting from 16 h before the failure. Prior to that point, in a scenario of near real-time monitoring, it may be considered difficult to extrapolate the exact shape and timing of the trend to failure.

4.2. Satellite InSAR data

Most of the failure area, including the slope sector above the pit crest invisible to the ground-based radar, is comprehensively covered by satellite InSAR data acquired in ascending geometry (Fig. 6). Such a dataset, thanks to the short satellite revisit time (up to 6 days in the latest part of the monitoring period), allows for the characterization of

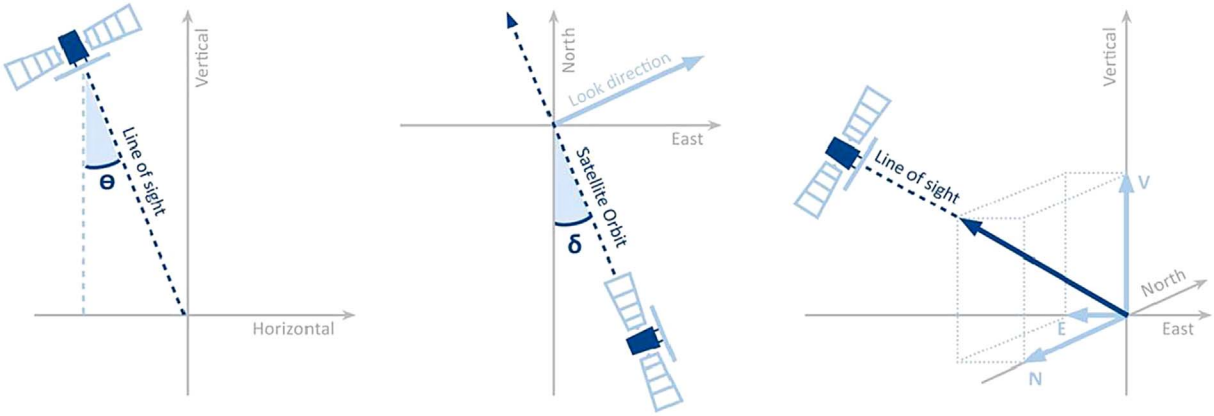

Fig. 8. Satellite looking angle in ascending orbit over the study area ($\theta = 39.22^{\circ}$; $\delta = 8.31^{\circ}$).

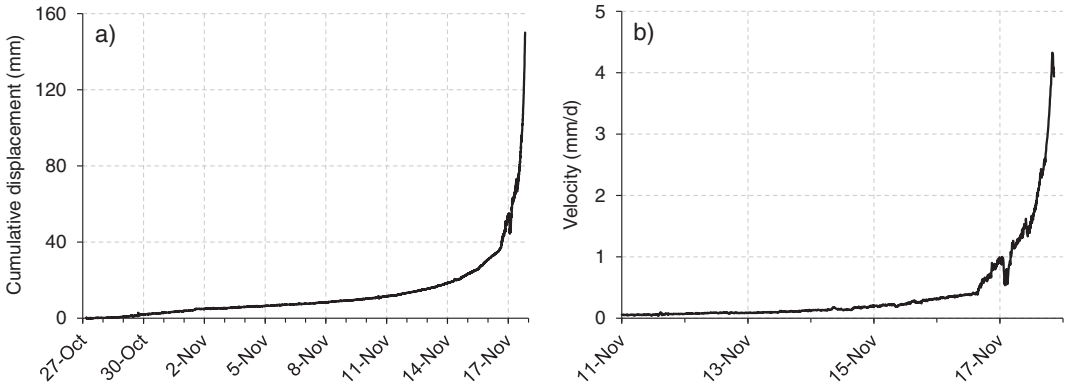

Fig. 9. (a) Average LOS cumulative displacement of the area in accelerating creep captured by the ground-based radar (white polygon in Fig. 5) and (b) corresponding velocity plot based on a 1-day running average of the data.

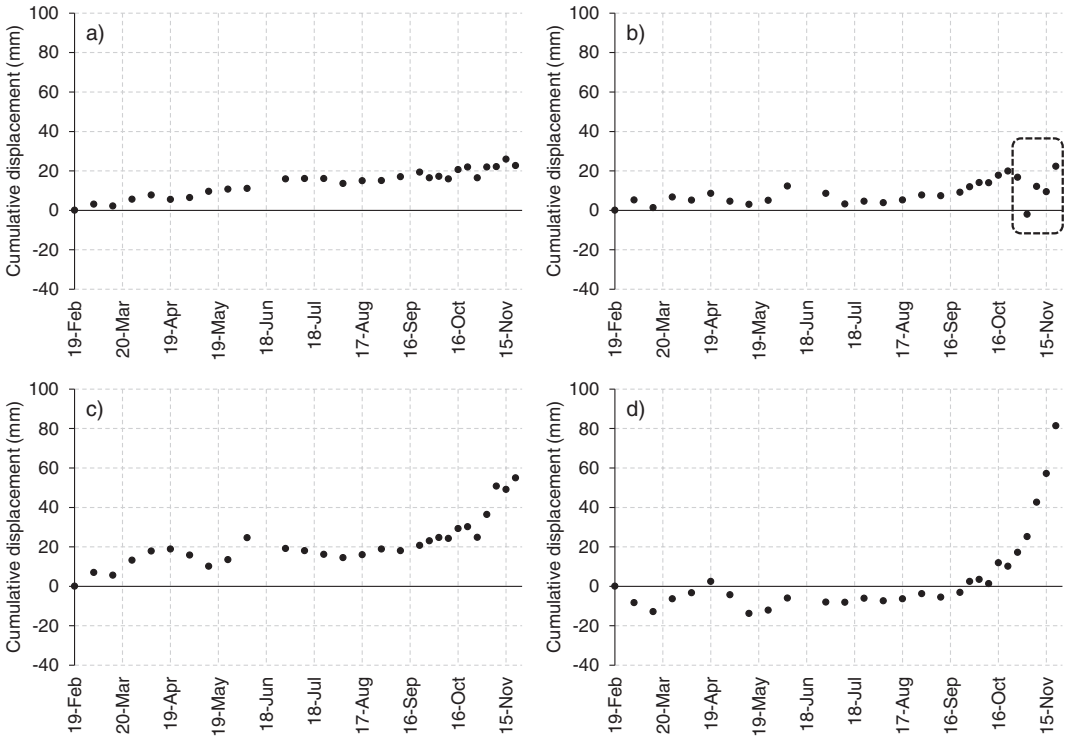

Fig. 10. Classification of the point scatterers in the ascending satellite InSAR dataset based on deformation behavior: (a) linear, (b) noisy/unclassifiable, (c) acceleration, and (d) accelerating creep.

the deformation trend with time of each measuring point, and consequently for the assessment of the spatial distribution of different slope behaviors. Point scatterers were distinguished according to 4 types of deformation trend, as exemplified in Fig. 10:

- Linear: no movement or constant velocity;
- Noisy/Unclassifiable: considerable scattering of the measurements in the time series. This may be related to noise or phase unwrapping, and makes uncertain the determination of the underlying deformation behavior (see points within the dashed polygon in Fig. 10);
- Acceleration: increase of velocity prior to the 17 November 2016 slope failure, however no definite evidence of progressive deformation;
- Accelerating creep: clear progressive deformation leading to the 17 November 2016 slope failure.

Fig. 11 shows the InSAR data within and in the surroundings of the failure, classified according to the aforementioned scheme. Those displaying accelerating creep are well clustered and spread over roughly 58,000 m^2, almost four times the respective area identified by the ground-based radar and more than half the extent of the total mapped area of the instability. Remarkably, the delimitation of such a clustering (white polygon in Fig. 11) matches well with both the detachment zone and most of the main accumulation zone of the failure. This suggests that the potential detachment zone, as created by the development of the main rupture surface, may have been partly overlain by the main accumulation zone, and therefore may actually extend more downslope than initially inferred from the change in topographic elevation along the slope (Fig. 2). The contrast between the targets displaying accelerating creep and those displaying linear deformation just outside of the failure boundaries is quite straightforward. No ambiguities in the data, such as those introduced in Fig. 5, were detected.

In Fig. 12 the displacement time series of the area in accelerating creep, derived by averaging all the point scatterers within the white polygon in Fig. 11, is shown. The lower entity of the movements derives

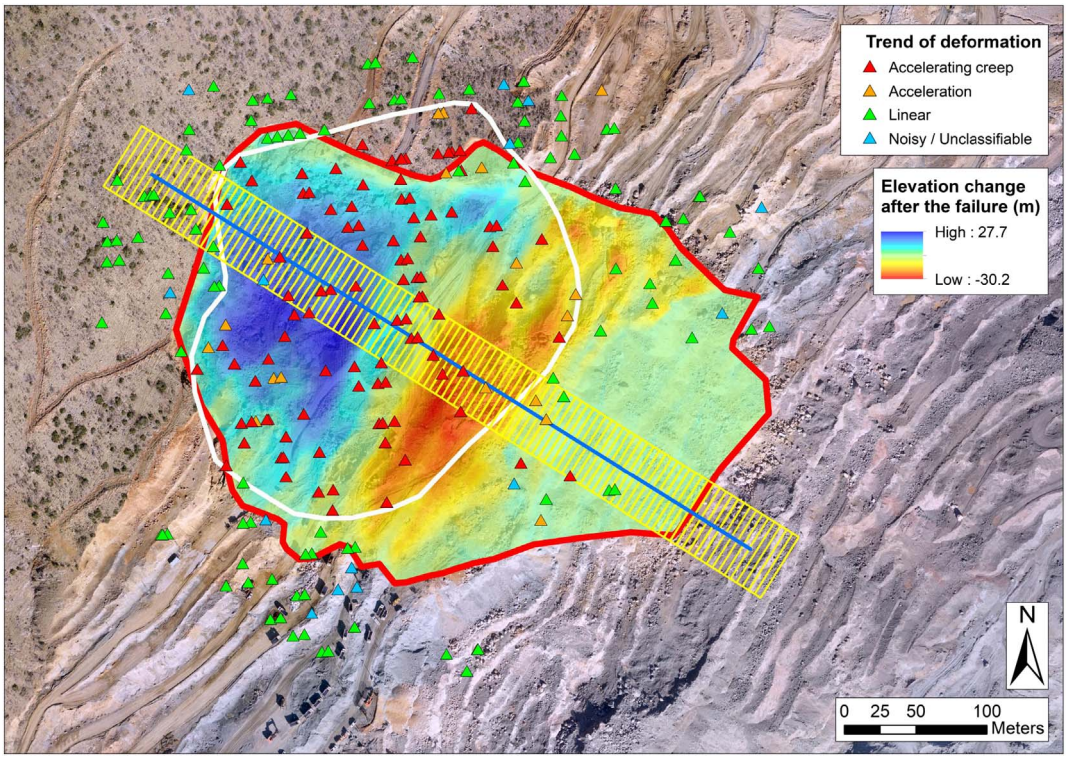

Fig. 11. Point scatterers within and in proximity of the failure, classified according to the deformation behavior. The blue line represents the trace of the cross-section in Fig. 14, the relative grid was used to derive the displacement profiles in Fig. 15 (see Section 5). (For interpretation of the references to color in this figure legend, the reader is referred to the web version of this article.)

from the more unfavorable LOS sensitivity of the satellite with respect to the ground-based radar (see Section 4.3). Given that the last flyover prior to the failure occurred before the final phase of rapid increase in slope velocity (as described in Fig. 9 and Section 4.1), and given the lower frequency of acquisition, the shape of the deformation trend is not as markedly exponential as that detected by the ground-based radar (note the different time scales between Figs. 9 and 12). The corresponding velocity plot relative to the acquisitions prior to the failure (i.e. up to 15 November 2016), based on a 3-measurement running average of the data, is characterized by LOS velocities > 1 mm/day starting from the 9 November 2016 acquisition. This indicates that the onset of the failure process may actually be collocated a few weeks earlier than what could be determined based on the available ground-based radar dataset.

4.3. Comparison of the datasets

Fig. 13 compares the satellite InSAR and radar datasets over the instability from late October up to the respective last acquisition prior to the failure. The displacements are corrected according to the LOS sensitivity to the actual direction of slope movement. The instability was assumed to move downslope according to the azimuth of its longitudinal axis, and with a vertical inclination equal to the average slope angle along such axis. As a result, a 93% and 79% LOS sensitivity was estimated for the radar and the satellite looking geometry, respectively. Finally, the radar displacements were resampled over a 10 × 10 m grid to account for the larger spatial resolution of the satellite data (5 × 15 m), thus making the comparison more meaningful.

The obvious discrepancy between the spatial coverage of the two datasets in the higher portion of the instability is once again evidenced. At the same time, more detail was obtained by the radar over the secondary accumulation zone. Fig. 13 also allows to assess that the

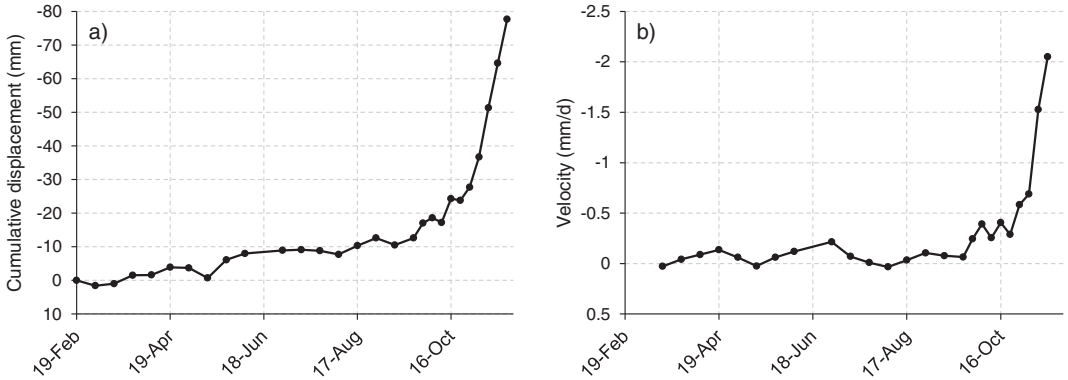

Fig. 12. (a) Average LOS cumulative displacement of the area in accelerating creep captured by the satellite InSAR during the entire monitoring period, and (b) corresponding velocity plot up to 15 November 2016 (last acquisition prior to the failure) based on a 3-measurement running average of the data.

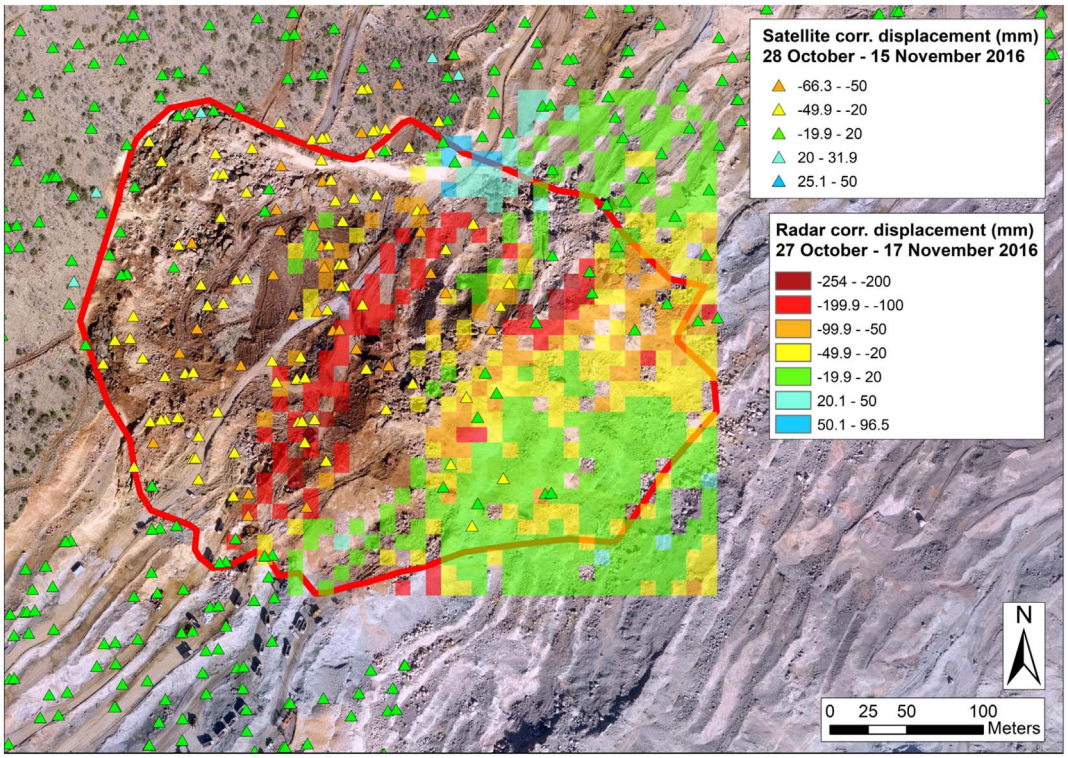

Fig. 13. Comparison between satellite InSAR and resampled radar data, corrected according to the respective LOS sensitivity. (For interpretation of the references to color in this figure legend, the reader is referred to the web version of this article.)

ambiguous radar data outlined in Fig. 5 and Section 4.1 can indeed be related to some kind of error, as in the same locations the satellite InSAR data show reasonable values of slope movement. The proximity to the limits of the slope coverage area, together with the presence of several voids in the deformation map, likely induced these artifacts in phase of data processing.

Some differences are also observed concerning the magnitude of the displacements, with ground-based radar measurements mostly displaying larger values. This may be explained by considering that the last acquisition prior to the failure in the satellite InSAR dataset was performed on 15 November 2016, and therefore the final part of the precursor acceleration (where most of the total displacement was concentrated) was not detected. Another factor may be a stronger horizontal component of actual slope movement than what was assumed for the LOS correction, which would result in a better LOS sensitivity of the radar with respect to the satellite. As prism surveys are not available, the evaluation of the actual direction of slope movement is necessarily a simplification.

5. Discussion

The unexpected nature of the large slope failure occurred on 17 November 2016 at an undisclosed copper open-pit mine prompted a thorough review of ground-based radar and satellite InSAR measurements of ground surface deformation acquired over the site. In recent years, attempts at integrating the two techniques have been limited, as satellite InSAR data could be mostly analyzed in terms of overall displacement/velocity and relative trends in the long term (Carlà et al., 2016b). The main constraint to the their use for slope failure identification and characterization was the inadequacy of a relatively low data temporal frequency for the high rates of displacement that typically develop rapidly in anticipation of such events. However, this gap is progressively being closed as technical advancements determine shorter satellite revisit time (up to 6 days in the case of the Sentinel-1 satellites for the study area) and faster processing of the interferometric images (Wasowski and Bovenga, 2014). Moreover, the increased number of measuring points that can be found on the ground by recent algorithms (e.g. including both Distributed and Persistent Scatterers according to SqueeSAR, as introduced by Ferretti et al., 2011) is important to assess the spatial distribution of the slope deformation trends in the short term.

The presented open-pit case study provides, to the knowledge of the authors, the first instance of accelerating creep behavior observed clearly and extensively by means of satellite InSAR on an open-pit slope approaching catastrophic failure. Since the analysis was conducted in retrospect, the suitability of the technique as a stand-alone prediction tool is still not demonstrated (see Section 5.5). The latter aspect represents the next logical step of research development. Nonetheless, the integration with monitoring data derived from a ground-based radar relative to the 3 weeks before the failure allowed to draw critical considerations on several features of the failure, and thus produced critical perspectives on the potential use of satellite InSAR in phase of early warning.

5.1. Estimation of rupture surface and failure proportions

Fig. 14 presents a slope cross-section along the profile trace outlined in Fig. 11, before and after the failure. The landslide length is also indicated. The point of intersection between the pre- and post-failure topography had been preliminarily associated with the approximate boundary between the detachment and main accumulation zones (see also Fig. 2). The rupture surface was in fact daylighting up to this point, and it was unclear, because of the thickness of the collapsed material, whether and how much it would persist further downslope below the main accumulation zone. The initial estimation of the failure volume (i.e. 410,000 m^3) was based only on the amount of material included in thus defined detachment zone, and considering an average sliding depth of 11 m.

The red shaded area in Fig. 14 marks the cross-section length of the slope sector displaying accelerating creep, as defined according to the

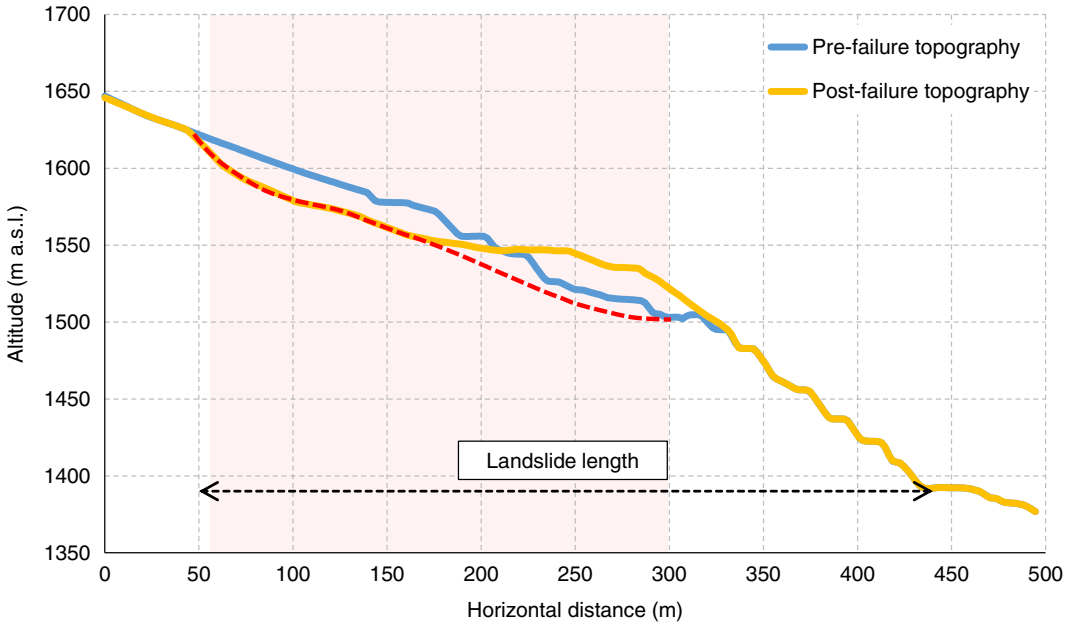

Fig. 14. Slope cross-section along the profile trace outlined in Fig. 11: the red shaded area includes the slope sector affected by accelerating creep, while the red dashed line indicates the inferred extension of the basal damage zone. (For interpretation of the references to color in this figure legend, the reader is referred to the web version of this article.)

intersection of the profile trace with the limits of the white polygon in Fig. 11. Since accelerating creep is supposed to affect those areas where rock fracture propagation and strain accumulation is occurring (Kemeny, 2003; Kilburn, 2012), it can be inferred that the basal damage zone, and consequently the potential detachment zone, extended downslope close to the lower boundary of the main accumulation zone (red dashed line in Fig. 14). This does not necessarily imply that, during the failure, material was mobilized over the entire slope sector under progressive deformation. Still, the estimation of the overall volume of the instability can be refined. Considering a spatial extent of 58,000 m^2 for the area in accelerating creep, and assuming the same average depth of the rupture surface that was defined for the upper part of the slope (i.e. 11 m), yields a volume of approximately 640,000 m^3. This is > 1.5 times the estimation derived from the comparison between the pre- and post-failure Digital Elevation Models. Most importantly, such proportions of the failure cannot be deduced with the available ground-based radar data (Fig. 5), which leads to substantial impacts in terms of expected run-out distance and perceived risk.

5.2. Temporal and spatial evolution of the displacements

The comprehensive coverage of satellite data gives the opportunity to determine how the failure process evolved in space and time. The profile trace in Fig. 11 consists of 100 nodes (spacing 5 m): each one of them is associated to a value of displacement for each date of satellite acquisition, calculated by averaging the measurements of all the point scatterers falling within a 50 × 50 m square centered on the node itself. LOS displacement profiles were consequently derived to describe how the deformation was distributed along the slope.

Fig. 15 shows the resulting LOS displacement profiles relatively to selected dates of satellite acquisition. Considering a 20 mm threshold of displacement, on 1 May 2016 a general condition of stability is still observed along the entire slope. The first event of deformation occurred in August between progressive distances 190 m and 280 m (sector 1), where most of the main accumulation zone will be identified after the failure (Fig. 2). The upper part of the slope had not yet experienced any relevant movement at this point (< 10 mm from start of monitoring). Definite deformation activity may in fact be observed between progressive distances 120 m and 170 m (sector 2) only in late October, with 30 mm of total measured displacement and an increase of 10 mm in just 6 days (i.e. from 22 to 28 October 2016). Together with the persistence of the acceleration in these two mentioned areas, profiles relative to 9 and 15 November 2016 highlight a further retrogression of the instability (i.e. up to progressive distance 80 m, sector 3) in the last days leading to failure. In overall terms, sectors 1, 2, and 3, experienced a cumulative LOS displacement of about 95, 70, and 50 mm, respectively.

The evolution of the displacements along the slope therefore suggests that the rupture surface generated at the base of the instability in correspondence of sector 1, and that it subsequently propagated and retrogressed upslope to the point of full development and sudden strength drop.

5.3. Role of rainfall as triggering factor

The larger temporal coverage of satellite InSAR data also allowed to analyze the long-term influence of precipitation on the displacement-time curve. Fig. 16 presents the average cumulative LOS displacement of the point scatterers affected by accelerating creep (as in Fig. 12) from July to November, compared to the daily rainfall that were registered by a pluviometer installed roughly 27 km NE of the mine at 1480 m of elevation. Among the available records, this pluviometer was deemed as the most representative of the atmospheric conditions at the mine site.

As mentioned in Section 4.2, the onset of acceleration in the satellite InSAR dataset may be collocated a few weeks earlier than what may be deduced solely from the ground-based radar measurements. In particular, this seemingly coincides with rainfall occurred in late September. A point of trend change in the displacements is then observed consistently with a major precipitation event spanning from late October to early November (170 mm of rainfall between 25 October and 2 November). Finally, another 12 mm rainfall characterized the overnight period between 16 and 17 November, and may have played the role of final trigger that prompted the failure. However, it is not possible to evaluate this event since it lies between the last acquisition prior to the failure (on 15 November 2016) and the failure itself. On the other hand, the level of detail of the ground-based radar data is able to shed light on the response of the slope to the last rainfall, whose occurrence indeed appears to be consistent with the onset of the final and abrupt increase in velocity that preceded the failure (Fig. 16).

The apparent dependency between rainfall and acceleration of the

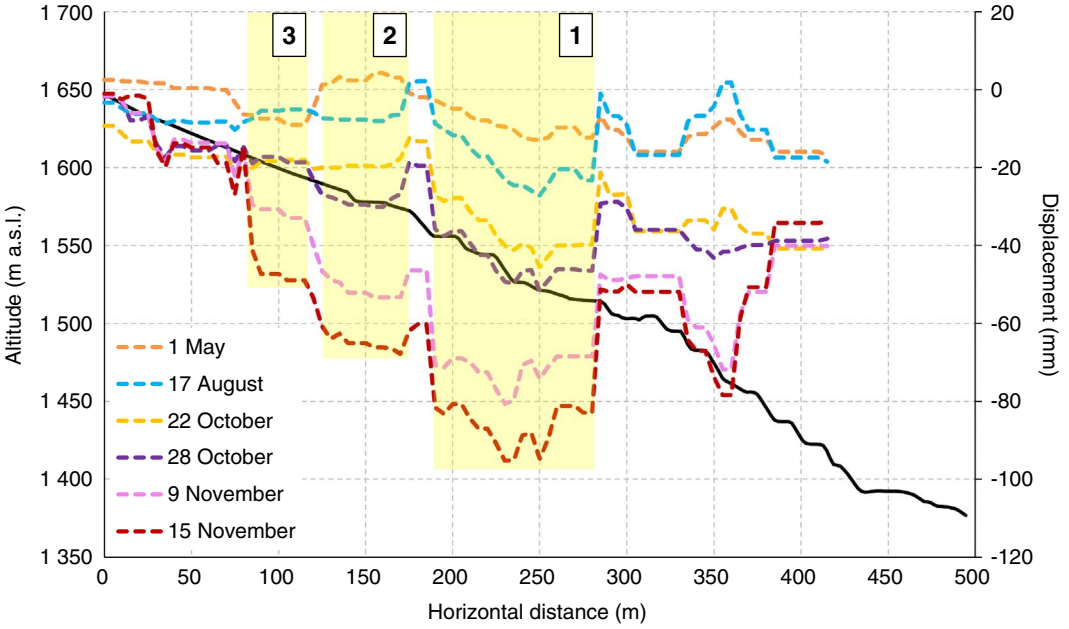

Fig. 15. LOS displacement profiles along the profile trace outlined in Fig. 11. The shaded areas highlight the slope sectors affected by deformation activity prior to the failure. (For interpretation of the references to color in this figure legend, the reader is referred to the web version of this article.)

displacements hints at the presence of water within the slope as the main driving factor of the instability. However, field measurements of pore pressure are not available and therefore no definitive conclusion can be drawn in this regard.

5.4. Failure predictability

The predictability of the failure was investigated by means of the inverse velocity method applied to the velocity plots presented in Figs. 9 and 12, respectively. Both the ground-based and satellite InSAR data are evidently characterized by a mostly linear trend leading to failure (Fig. 17). This is in accordance with a slope instability developing through the nucleation of a new rupture surface, where movement is dominantly caused by time-dependent mechanisms of crack propagation and degradation of rock joint cohesion (Petley et al., 2002; Kemeny, 2003), and therefore also with the hypothesized retrogression of the failure (Section 5.2).

Remarkably, despite the poorer temporal frequency of the measurements, linear regression of the inverse velocity plot based on satellite InSAR data is of high quality (R^2 = 0.86) and, in retrospect, provides an excellent prediction of the time of failure. Such trend may be considered identifiable since early November. Excellent prediction is obtained through the ground-based radar data as well: the last part of the relative inverse velocity plot is clearly indicative of a forthcoming event of slope failure, and is comparable to reference case studies reported in the literature concerning the use of the method (e.g. Rose and Hungr, 2007; Dick et al., 2015). The greater temporal resolution also determines more confidence in phase of prediction, at the cost of increased data noise when slope velocity is still limited. As a result the final trend to failure may be considered evident from approximately 5–6 days before the event, which is considerably later (roughly 10 days) than what observed in the satellite InSAR data. In this sense, it is stressed that increasing the potential to detect the final trend to failure with larger notice would have crucial repercussions for any effective early warning strategy.

Using ground-based radar measurements smoothed over a shorter time interval to obtain an earlier onset of acceleration yields no benefit because of the large amount of noise in the time series. This is made explicit in Fig. 18, where data are averaged and reduced to one measurement per day and per hour, respectively. In the first case the final trend is observed at least from 12 November 2016, whereas in 1-hour data this can be extrapolated only in the last 7–8 h and generates a slightly delayed prediction (almost 2 h) with respect to the actual failure-time.

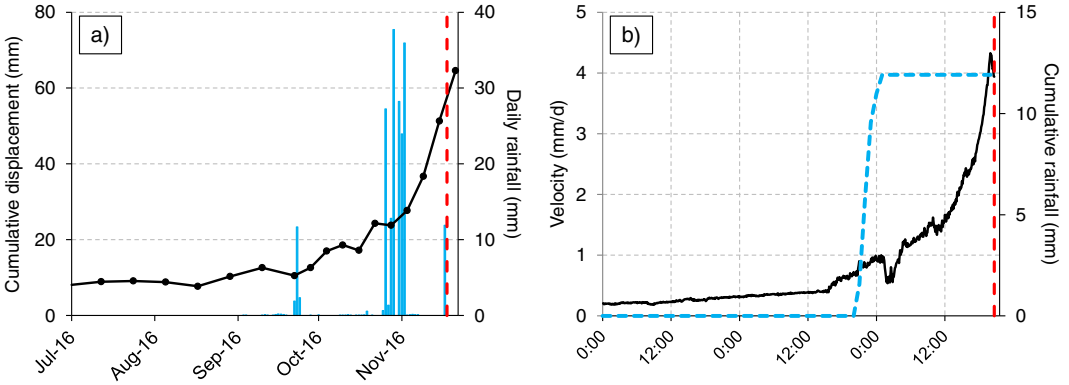

Fig. 16. (a) Average cumulative LOS displacement of the area in accelerating creep captured by the satellite InSAR from July to November, compared to the daily rainfall. (b) Average LOS velocity of the area in accelerating creep captured by the ground-based radar from 15 to 17 November 2016, compared to the cumulative rainfall.

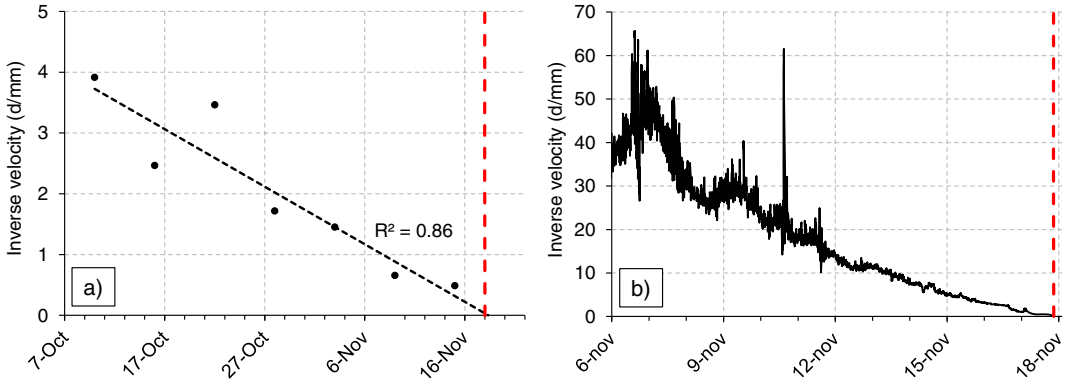

Fig. 17. (a) Inverse velocity analysis of the satellite InSAR data, as derived from the velocity plot in Fig. 12, and (b) inverse velocity analysis of the ground-based radar data, as derived from the velocity plot in Fig. 9. In each plot, the red dashed line marks the failure-time. (For interpretation of the references to color in this figure legend, the reader is referred to the web version of this article.)

5.5. Remarks on the complementarity between ground-based radar and satellite InSAR techniques to identify and characterize impending catastrophic slope failures

Ground-based radar has proved to be one of the cutting-edge techniques for the timely detection of slope failures in both natural and engineered slopes, thanks to its accuracy, frequency, and resolution of measurement. However, some constraints may occasionally be induced by an inadequate field of view of the instrument. The latter aspect was crucial in the case of the presented open-pit slope failure, as the main reason behind the fatality of the event has been the impossibility to perceive its actual proportions from the poor radar coverage over the unstable area. In fact, most of the detachment zone was located above the upper limit of the mine and was therefore outside of the radar deformation map. Since the available data were affected by a large amount of noise due to the ongoing production works, long-term smoothing would have also been needed in order to highlight the fundamental trend to failure (Figs. 17 and 18).

On the other hand, satellite InSAR data acquired by the Sentinel-1 satellites over the study area were not affected by such limitation, as the overview looking geometry meant that there were no shadow areas above the pit crest (Fig. 6). A lack of coverage concerned only the bottom sector of the pit. Moreover, they provided, to the knowledge of the authors, the first clear example of slope accelerating creep leading to catastrophic failure in an open-pit mine captured with such technique. This may be deemed a direct consequence of the increased revisit time of modern satellites, which guaranteed one measurement of ground displacements every 6 days in the last part of the dataset. In light of the large number of point scatterers that can be identified on the ground by modern processing algorithms of satellite interferometric images (e.g. SqueeSAR), accelerating creep was observed comprehensively across the entire slope sector that was affected by the failure. This allowed to estimate the volume of the unstable mass and the rupture surface extent, along with the possible retrogression of the failure over time.

The results evidenced the complementarity of the two techniques for the monitoring of slopes prone to catastrophic failure. Given the current state of the art, notice of a future failure may be obtained "qualitatively" with satellite InSAR, and "quantitatively" with ground-based radar. In particular, with regard to the presented case study: while the satellite InSAR dataset showed a long-term accelerating trend typical of an ongoing slope failure process and an accurate description of its size, in practice it would have not been useful to support short-term forecasting. Such a dataset was in fact used, in retrospect, to derive an accurate failure-time prediction by means of the inverse velocity method (Fig. 17), but a revisit time of 6 days may still not be sufficient for an early warning system that is supposed to work in near real-time. The sensitivity to rapid movements is also further decreased when taking into account the time that is necessary to acquire and process stacks of images for multi-interferogram analyses. Conversely the ground-based radar dataset, despite limitations concerning the possibility to identify the full size of the instability, had a temporal resolution able to closely follow the evolution of the precursor deformation phase. Given adequate data processing, this would have provided a reliable failure-time estimation a few days before the failure.

6. Conclusions

Different types of slope monitoring systems have been successfully developed, and ground-based radar is among the current cutting-edge techniques. However, any terrestrial instrument may present some limitations in terms of the size of the covered area with respect to the

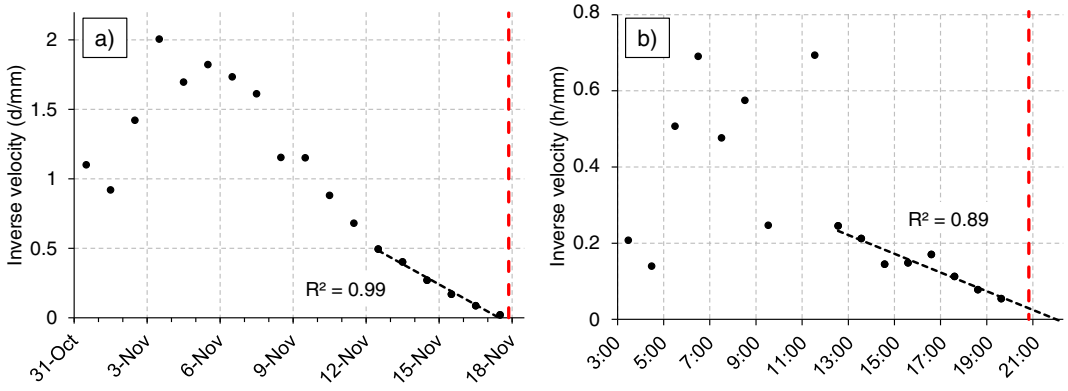

Fig. 18. Inverse velocity analysis of the ground-based radar data averaged to (a) one measurement per day and (b) one measurement per hour, respectively.

overview looking geometry of satellite sensors. This proved to be a key factor for the unexpected nature of the presented open-pit slope failure, as the ground-based radar was not able to detect displacements above the mine crest, where most of the detachment zone was located. In relation to the analysis of slope movements, most applications of satellite InSAR measurements have concerned landslide mapping and susceptibility assessment. This was mainly due to the low frequency of acquisition, which put unavoidable constraints to the detection of high rates of deformation. The shortened revisit time of modern satellites now offers the opportunity to overcome this issue, and to use satellite InSAR data to identify and characterize impending slope failures.

In retrospect, crucial insights were gained concerning the spatial properties and the long-term deformation trend of the open-pit failure case study, mainly thanks to the ability of the satellite to capture displacements above the pit crest every 6 days. Clear accelerating creep behavior, involving the entire source area of the instability, was detected for the first time in an open-pit mine with satellite InSAR data. This allowed to derive critical considerations on the volume of the failure and on the retrogression with time of the rupture surface. It was also observed that near real-time early warning can be obtained only through data of very high temporal resolution. Measurements provided by the ground-based radar were ideal to confidently extrapolate short-term predictions through the inverse velocity method and to detail the response of the instability to the last rainfall event.

The results underline the complementarity between ground-based and satellite radar interferometry, and the advantages that can potentially be gained by integrating the two techniques for the monitoring of slopes prone to catastrophic failure.

References

Antonello, G., Casagli, N., Farina, P., Leva, D., Nico, G., Sieber, A.J., Tarchi, D., 2004. Ground-based SAR interferometry for monitoring mass movements. Landslides 1 (1), 21–28.

Armstrong, J., Rose, N.D., 2009. Mine operation and management of progressive slope deformation on the south wall of the Barrick Goldstrike Betze-Post Open Pit. In: Proceedings of Slope Stability 2009: International Symposium on Rock Slope Stability in Open Pit Mining and Civil Engineering. Santiago, Chile; 9–11 November.

Atzeni, C., Barla, M., Pieraccini, M., Antolini, F., 2015. Early warning monitoring of natural and engineered slopes with ground-based synthetic-aperture radar. Rock Mech. Rock. Eng. 48 (1), 235–246.

Bardi, F., Frodella, W., Ciampalini, A., Bianchini, S., Del Ventisette, C., Gigli, G., Fanti, R., Moretti, S., Basile, G., Casagli, N., 2014. Integration between ground based and satellite SAR data in landslide mapping: the San Fratello case study. Geomorphology 223, 45–60.

Berardino, P., Costantini, M., Franceschetti, G., Iodice, A., Pietranera, L., Rizzo, V., 2003. Use of differential SAR interferometry in monitoring and modelling large slope instability at Maratea (Basilicata, Italy). Eng. Geol. 68 (1–2), 31–51.

Carlà, T., Intrieri, E., Di Traglia, F., Nolesini, T., Gigli, G., Casagli, N., 2016a. Guidelines on the use of inverse velocity method as a tool for setting alarm thresholds and forecasting landslides and structure collapses. Landslides 14 (2), 517–534.

Carlà, T., Raspini, F., Intrieri, E., Casagli, N., 2016b. A simple method to help determine landslide susceptibility from spaceborne InSAR data: the Montescaglioso case study. Environ. Earth Sci. 75 (24), 1492.

Casagli, N., Catani, F., Del Ventisette, C., Luzi, G., 2010. Monitoring, prediction, and early warning using ground-based radar interferometry. Landslides 7 (3), 291–301.

Casagli, N., Frodella, W., Morelli, S., Tofani, V., Ciampalini, A., Intrieri, E., Raspini, F., Rossi, G., Tanteri, L., Ping, L., 2017. Spaceborne, UAV and ground-based remote sensing techniques for landslide mapping, monitoring and early warning. Geoenviron. Disasters 4 (9), 1–23.

Catani, F., Casagli, N., Ermini, L., Righini, G., Menduni, G., 2005. Landslide hazard and risk mapping at catchment scale in the Arno River basin. Landslides 2 (4), 329–342.

Cigna, F., Bianchini, S., Casagli, N., 2013. How to assess landslide activity and intensity with Persistent Scatterer Interferometry (PSI): the PSI-based matrix approach. Landslides 10 (3), 267–283.

Colesanti, C., Wasowski, J., 2006. Investigating landslides with space-borne Synthetic Aperture Radar (SAR) interferometry. Eng. Geol. 88 (3–4), 173–199.

Corsini, A., Farina, P., Antonello, G., Barbieri, M., Casagli, N., Coren, F., Guerri, L., Ronchetti, F., Sterzai, P., Tarchi, D., 2006. Space-borne and ground-based SAR interferometry as tools for landslide hazard management in civil protection. Int. J. Remote Sens. 27, 2351–2369.

Crosetto, M., Monserrat, O., Cuevas-González, M., Devanthéry, N., Crippa, B., 2016. Persistent Scatterer Interferometry: a review. ISPRS J. Photogramm. 115, 78–89.

Crosta, G.B., Agliardi, F., 2003. Failure forecast for large rock slides by surface displacement measurements. Can. Geotech. J. 40, 176–191.

Crosta, G.B., Agliardi, F., Rivolta, C., Alberti, S., Dei Cas, L., et al., 2017. Landslides. http://dx.doi.org/10.1007/s10346-017-0817-8.

Dick, G.J., Eberhardt, E., Cabrejo-Liévano, A.G., Stead, D., Rose, N.D., 2015. Development of an early-warning time-of-failure analysis methodology for open-pit mine slopes utilizing ground-based slope stability radar monitoring data. Can. Geotech. J. 52, 515–519.

Doyle, J.B., Reese, J.D., 2011. Slope monitoring and back analysis of east fault failure, Bingham Canyon Mine, Utah. In: Proceedings of Slope Stability 2011: International Symposium on Rock Slope Stability in Open Pit Mining and Civil Engineering. Vancouver, Canada; 18–21 September.

Eberhardt, E., 2008. The role of advanced numerical methods and geotechnical field measurements in understanding complex deep-seated rock slope failure mechanisms. Can. Geotech. J. 45 (4), 484–510.

Espinosa, E.A.E., Farina, P., Leoni, L., Iasio, C., Coli, N., 2013. Innovative use of slope monitoring radar as a support to geotechnical modeling of slopes in open pit mines. In: Proceedings of the 2013 International Symposium on Rock Slope Stability in Open Pit Mining and Civil Engineering. Brisbane, Australia; 25–27 September.

Farina, P., Colombo, D., Fumagalli, A., Marks, F., Moretti, S., 2006. Permanent Scatterers for landslide investigations: outcomes from the ESA-SLAM project. Eng. Geol. 88 (3–4), 200–217.

Farina, P., Coli, N., Yön, R., Eken, G., Keitzmen, H., 2013. Efficient real time stability monitoring of mine walls: the Çöllolar Mine Case Study. In: Proceedings of the 23rd International Mining Congress & Exhibition of Turkey. Antalya, Turkey; 16–19 April, pp. 111–117.

Farina, P., Coli, N., Coppi, F., Babboni, F., Leoni, L., Marques, T., Costa, F., 2014. Recent advances in slope monitoring radar for open-pit mines. In: Proceedings of Mine Closure Solutions 2014. Ouro Preto, Minas Gerais, Brazil; 27–30 April.

Federico, A., Popescu, M., Elia, G., Fidelibus, C., Internò, G., Murianni, A., 2012. Prediction of time to slope failure: a general framework. Environ. Earth Sci. 66, 245–256.

Ferretti, A., Fumagalli, A., Novali, F., Prati, C., Rocca, F., Rucci, A., 2011. A new algorithm for processing interferometric data-stacks: SqueeSAR. IEEE Trans. Geosci. Rem. Sen. 49 (9), 3460–3470.

Frodella, W., Ciampalini, A., Gigli, G., Lombardi, L., Raspini, F., Nocentini, M., Scardigli, C., Casagli, N., 2016. Synergic use of satellite and ground based remote sensing methods for monitoring the San Leo rock cliff (Northern Italy). Geomorphology 264, 80–94.

Fukuzono, T., 1985. A new method for predicting the failure time of a slope. In: Proceedings of the 4th International Conference and Field Workshop on Landslides. Tokyo, Japan, pp. 145–150.

Herrera, G., Fernández-Merodo, J.A., Mulas, J., Pastor, M., Luzi, G., Monserrat, O., 2009. A landslide forecasting model using ground based SAR data: the Portalet case study. Eng. Geol. 105 (3–4), 220–230.

Herrera, G., Notti, D., García-Davalillo, J.C., Mora, O., Cooksley, G., Sánchez, M., Arnaud, A., Crosetto, M., 2011. Analysis with C- and X-band satellite SAR data of the Portalet landslide area. Landslides 8 (2), 195–206.

Hilley, G.E., Bürgmann, R., Ferretti, A., Novali, F., Rocca, F., 2004. Dynamics of slow-moving landslides from Permanent Scatterer analysis. Science 304 (5679), 1952–1955.

Intrieri, E., Gigli, G., 2016. Landslide forecasting and factors influencing predictability. Nat. Hazards Earth Syst. Sci. 16, 2501–2510.

Intrieri, E., Raspini, F., Fumagalli, A., Lu, P., Del Conte, S., Farina, P., Allievi, J., Ferretti, A., Casagli, N., 2017. The Maoxian landslide as seen from space: detecting precursors of failure with Sentinel-1 data. Landslides. http://dx.doi.org/10.1007/s10346-017-0915-7.

Kemeny, J., 2003. The time-dependent reduction of sliding cohesion due to rock bridges along discontinuities: a fracture mechanics approach. Rock Mech. Rock. Eng. 36 (1), 27–38.

Kilburn, C., 2012. Precursory deformation and fracture before brittle rock failure and potential application to volcanic unrest. J. Geophys. Res. 117, B02211.

Komac, M., Holley, R., Mahapatra, P., Van der Marel, H., Bavec, M., 2015. Coupling of GPS/GNSS and radar interferometric data for a 3D surface displacement monitoring of landslides. Landslides 12 (2), 241–257.

Luzi, G., Pieraccini, M., Mecatti, D., Noferini, L., Macaluso, G., Galgaro, A., Atzeni, C., 2006. Advances in ground based microwave interferometry for landslide survey: a case study. Int. J. Remote Sens. 27 (12), 2331–2350.

Michoud, C., Bazin, S., Blikra, L.H., Derron, M.H., Jaboyedoff, M., 2013. Experiences from site-specific landslide early warning systems. Nat. Hazards Earth Syst. Sci. 13 (10), 2659–2673.

Monserrat, O., Crosetto, M., Luzi, G., 2014. A review of ground-based SAR interferometry for deformation measurement. ISPRS J. Photogramm. 93, 40–48.

Petley, D.N., Bulmer, M.H., Murphy, W., 2002. Patterns of movement in rotational and translational landslides. Geology 30 (8), 719–722.

Petley, D.N., Mantovani, F., Bulmer, M.H., Zannoni, A., 2005. The use of surface monitoring data for the interpretation of landslide movement patterns. Geomorphology 66, 133–147.

Raspini, F., Bardi, F., Bianchini, S., Ciampalini, A., Del Ventisette, C., Farina, P., Ferrigno, F., Solari, L., Casagli, N., 2017. The contribution of satellite SAR-derived displacement measurements in landslide risk management practices. Nat. Hazards 86 (1), 327–351.

Read, J., Stacey, P., 2009. Guidelines for Open Pit Slope Design. CSIRO Publishing, Collingwood, Australia.

Righini, G., Del Ventisette, C., Costantini, M., Malvarosa, F., Minati, F., 2008. Space-borne SAR analysis for landslides mapping in the framework of the PREVIEW project. In: Proceedings of the 1st World Landslide Forum. Tokyo, Japan; 18–21 November, pp. 18–21.

Rose, N.D., Hungr, O., 2007. Forecasting potential rock slope failure in open pit mines

using the inverse velocity method. Int. J. Rock Mech. Min. Sci. 44, 308–320.
Sornette, D., Helmstetter, A., Andersen, J.V., Gluzman, S., Grasso, J.-R., Pisarenko, V., 2004. Towards landslide predictions: two case studies. Physica A. 338, 605–632.
Strozzi, T., Farina, P., Corsini, A., Ambrosi, C., Thuring, M., Zilger, J., Wiesmann, A., Wegmuller, U., Werner, C., 2005. Survey and monitoring of landslide displacements by means of L-band satellite SAR interferometry. Landslides 2 (3), 193–201.
Tarchi, D., Casagli, N., Fanti, R., Leva, D., Luzi, G., Pasuto, A., Pieraccini, M., Silvano, S., 2003. Landslide monitoring by using ground-based SAR interferometry: an example of application to the Tessina landslide in Italy. Eng. Geol. 68 (1–2), 15–30.
Tofani, V., Raspini, F., Catani, F., Casagli, N., 2013. Persistent Scatterer Interferometry (PSI) technique for landslide characterization and monitoring. Remote Sens. 5 (3), 1045–1065.
Vaziri, A., Moore, L., Ali, H., 2010. Monitoring systems for warning impending failures in slopes and open pit mines. Nat. Hazards 55 (2), 501–512.
Voight, B., 1988. A method for prediction of volcanic eruptions. Nature 332, 125–130.
Voight, B., 1989. A relation to describe rate-dependent material failure. Science 243, 200–203.
Wasowski, J., Bovenga, F., 2014. Investigating landslides and unstable slopes with satellite Multi Temporal Interferometry: current issues and future perspectives. Eng. Geol. 174, 103–138.
Zavodni, Z.M., Broadbent, C.D., 1978. Slope failure kinematics. In: Proceedings of the 19th U.S. Symposium on Rock Mechanics (USRMS). Reno, Nevada (USA); 1–3 May.